Frontiers: Laser Driven Accelerators

Motivation

Tabletop plasma accelerators can now produce GeV-range electron beams[1–5] and femtosecond X-ray pulses[6], providing compact radiation sources for medicine, nuclear engineering, materials science and high-energy physics[7]. In these accelerators, electrons surf on electric fields exceeding 100 GeV m^{-1}, which is more than 1,000 times stronger than achievable in conventional accelerators.

Matlis et al Nature Phys 2, 749 (2006)

- Cost, convenience and Science
- RF accelerators limited by material breakdown to ~100 MV/m
    - plasmas are already broken down. No walls!
- Plasma wake fields > 100 GV/m. Three orders of magnitude enhancement
    - compact, cheap compared to RF accelerators
    - potential for brighter electron beams with shorter bunch lengths
- Broaden applications of accelerators
    - cancer therapy, ion implantation, electron beam cutting and melting, non-destructive inspection
- Femtosecond electron pulses
    - femtochemistry
    - biochemistry of radiation damage

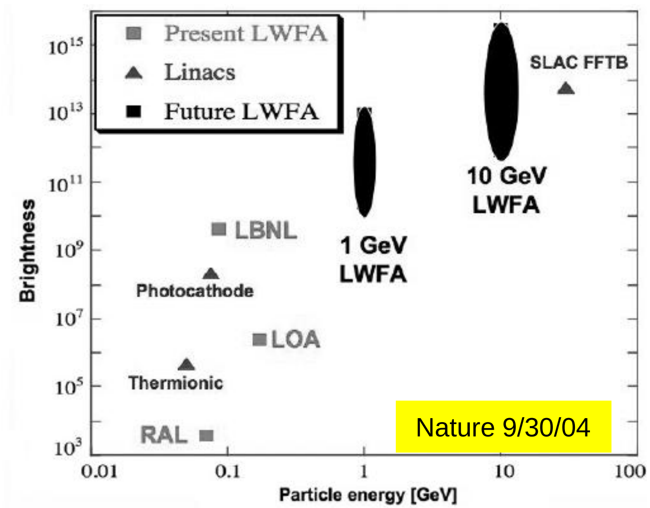

Fig. 4. Electron Beam Brightness Vs. Particle Energy for a Conventional Thermionic Gun, a Photocathode RF Gun, the SLAC FFTB Beam, Beams Reported in the September 30, 2004 *Nature Issue*, and Expected Performance of a 1 GeV and a 10 GeV Laser Driven Accelerator. The Brightness is Calculated by Multiplying the Total Number of Particles with the Mean Bunch Energy and Dividing by the Bunch Duration, the Relative Energy Spread and the Square of the Unnormalized Emittance (in mm^2-$mrad^2$)

Laser Wakefield Accceleration

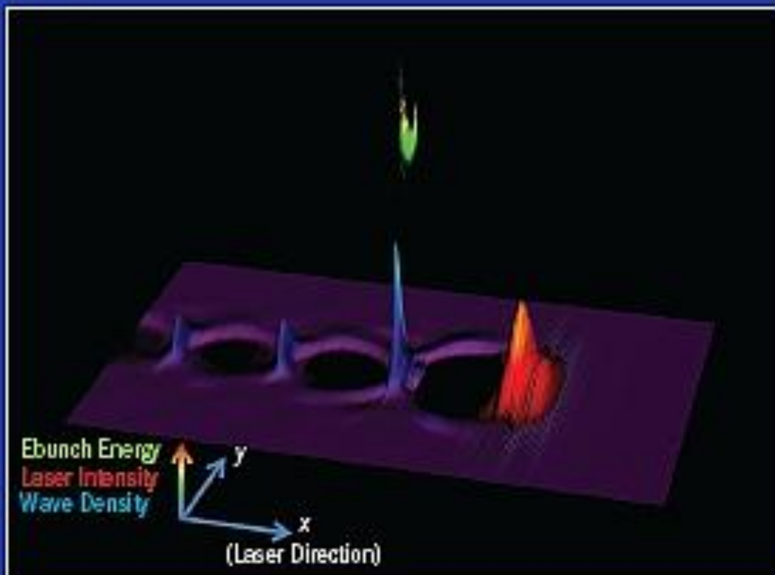

- radiation pressure from optical pulse (red) separates e- from heavier ions
- the displacement creates a density wave (purple-blue)
- the electric field from the density wave accelerates particles (green-yellow)
- similarly, the speedboat creates a wake that can move a surfer

http://www.scidacreview.org/0903/html/geddes.html

Laser Fields and scaling

Write the laser field in terms of the vector potential **A**

$$\mathbf{E} = -\frac{\partial \mathbf{A}}{c\partial t}, \quad \mathbf{B} = \nabla \times \mathbf{A}$$

Define the normalized vector potential as

$$\mathbf{a} = \frac{e\mathbf{A}}{m_e c^2}$$

And the **laser strength parameter** is given by

$$a_0 = \left(\frac{2e^2 \lambda_0^2 I}{\pi m_e^2 c^5}\right)^{1/2} \cong 0.855 \times 10^{-9} I^{1/2} \left[\mathrm{W/cm^2}\right] \lambda_0 [\mu\mathrm{m}]$$

I: laser peak intensity, λ is the wavelength

The amplitude of the transverse electric field of linearly polarized laser is

$$E_L[\mathrm{TV/m}] = \frac{m_e c^2 k}{e} a_0 \cong 3.21 \frac{a_0}{\lambda[\mu\mathrm{m}]} \cong 2.7 \times 10^{-9} I^{1/2} \left[\mathrm{W/cm^2}\right]$$

At $I = 1 \times 10^{18}$ W/cm^2, $\mathrm{E_L} = 2.7$ TV/m

E. Esary, LBNL Report, LBNL-53510, 2003

Lawson-Woodward theorem

There is no net energy gain for an electron when interacting with a laser field

- Laser field in vacuum, no boundaries or walls
- The electron is highly relativistic, $\beta \to 1$
- No static E or B field in presence
- Region of interaction is infinite

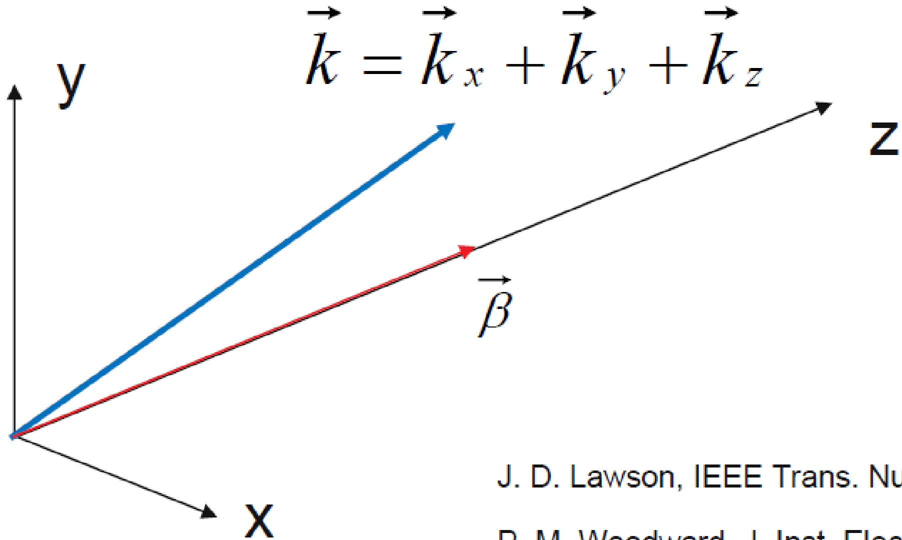

J. D. Lawson, IEEE Trans. Nucl. Sci. NS-26, 4217 (1979).

P. M. Woodward, J. Inst. Electr. Eng. **93**, 1554 (1947).

Lawson-Woodward theorem

An electron propagating in z is accelerated by E_z, and in vacuum this is

$$E_z = \frac{1}{2\pi}\int dk_x \int dk_y \hat{E}_z(k_x, k_y)\exp\left[i(k_x x + k_y y + k_z z - \omega t)\right]$$

In vacuum, one has

$$k_z = \sqrt{(\omega/c)^2 - k_x^2 - k_y^2}, \quad k = \omega/c$$

Field in Fourier space

$$\hat{E}_z = -\frac{1}{k_z}\left(k_x \hat{E}_x + k_y \hat{E}_y\right) \longleftarrow \nabla\cdot\vec{E} = 0 \Rightarrow k_z\hat{E}_z + k_x\hat{E}_x + k_y\hat{E}_y = 0$$

Assuming linear polarization along x, and the electron propagate along z with x=y=0, thus

$$\hat{E}_z = -\frac{1}{k_z}\left(k_x \hat{E}_x + k_y \hat{E}_y\right) = -\frac{k_x}{k_z}\hat{E}_x$$

$$\exp\left[i(k_x x + k_y y + k_z z - \omega t)\right] = \exp\left[i(k_z z - \omega t)\right]$$

$$\vec{k} = \vec{k}_x + \vec{k}_y + \vec{k}_z$$

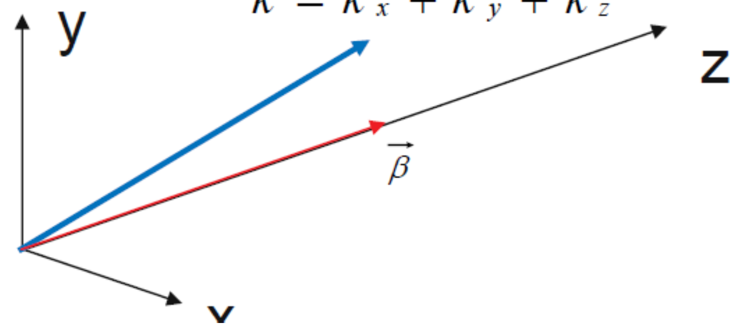

Yuelin Li, USPAS 2008

Lawson-Woodward theorem

Assuming linear polarization along x, and the electron propagate along z with x=y=0, thus the energy gain is

$$\Delta U = q\int E_z dz = \frac{q}{2\pi}\int dk_x \int dk_y \frac{k_x}{k_z}\hat{E}_x(k_x,k_y)\int dz \exp[i(k_z z-\omega t)]$$

If there is no boundary and the integration for z is on infinity

$$\int_{-\infty}^{\infty} dz \exp[i(k_z z-\omega t)] = \delta(k_z - k)$$

$$k_z z - \omega t = k_z z - kct = (k_z - k)z$$

$$\Rightarrow \Delta U = q\int_{-\infty}^{\infty} E_z dz = \frac{q}{2\pi}\int dk_x \int dk_y \frac{k_x}{k_z}\hat{E}_x(k_x,k_y)\delta(k_z - k)$$

Clearly, $\delta(k_z - k) \neq 0$ only when $k_z = k$, then $k_x = 0$. Thus under this condition

$$\Rightarrow \Delta U = q\int_{-\infty}^{\infty} E_z dz = 0$$

Lawson-Woodward theorem

The physical root behind Lawson-Woodward is the slippage that the electron undergoes because the phase velocity of the longitudinal field is superluminal, so integrated over infinite length, absent nonlinear effects, matter, inhomogeneous optical field, or external fields, you can't get any energy from the direct field.

- Gee, that's a pretty long list of exceptions

- Finite length ('semi-vacuum'). Plettner et al, PRL 95, 134801 (2005).
    - 30 keV modulation on 30 MeV beam
- Add gas, reduce phase velocity v_{ph} . Kimura et al PRL 74, 546 (1995)
    - 3.7 MeV on 40 MeV beam
    - add guiding (self-focusing). Sprangle et al PRE 54, 4211 (1996)
    - ionization increases v_{ph}
- Use an external B field: that's an IFEL
- Use the ponderomotive force $d\tilde{\boldsymbol{p}}/dct = \partial \boldsymbol{a}/\partial ct - \boxed{(\tilde{\boldsymbol{p}}/\tilde{\gamma}) \times (\nabla \times \boldsymbol{a})}$

E. Esarey et al, RevModPhys 81, 1229 (2009)

Semi-vacuum

- For a Gaussian beam propagating along z', and electron propagating along z

$$E_\perp(x',y',z',t) = \frac{E_0}{\sqrt{1+(z'/z_0)^2}} \exp\left[-\frac{x'^2+y'^2}{w(z')^2}\right] \exp\left\{ i\left[\omega t - kz' - \eta(z') - \frac{kx'^2}{2R(z')} - \varphi\right]\right\}$$

$$z_0 = \pi\frac{w_0^2}{\lambda},\ w(z') = w_0\left[1+(z'/z_0)^2\right],\ R(z') = z\left[1+(z'/z_0)^2\right],\ \eta(z') = \tan^{-1}(z'/z_0)$$

- The field along z' is, obtained from Gauss's law, $\nabla \cdot \vec{E} = 0$

$$E_{z'}(x',z') = -2x'\left[\frac{1}{w(z')^2} + \frac{ik}{2R(z')}\right] E_{x'}(z')$$

- The field along z

$$E_z(z) = E_{z'}\cos\alpha + E_{x'}\sin\alpha$$

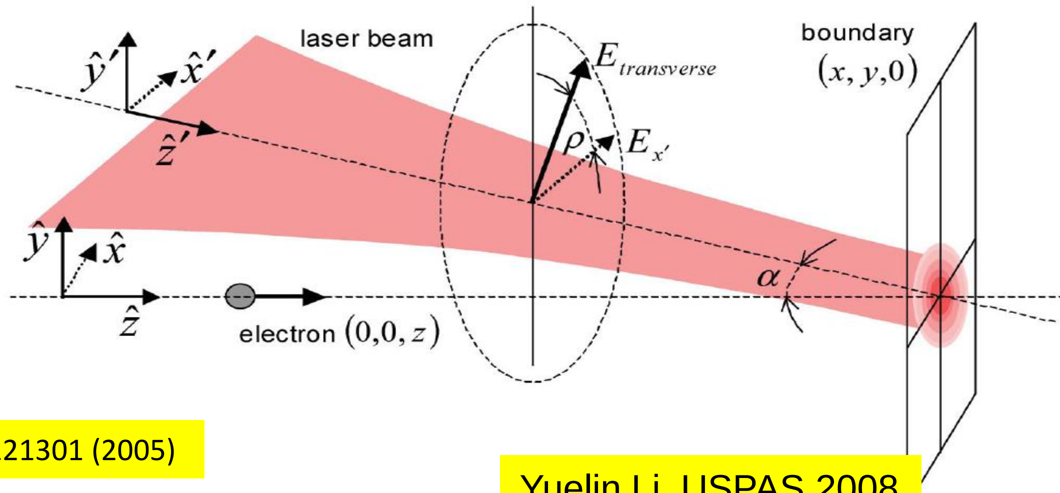

T. Plettner et al., PRL 95, 134801 (2005); PRSTAB 8, 121301 (2005)

B She

Yuelin Li, USPAS 2008

Semi-vacuum

- The energy gain of the electron

$$\Delta U = \int_{-\infty}^{0} qE_z(z)dz \sim \frac{\lambda e E_0}{\pi}\frac{\alpha}{\alpha^2 + 1/\gamma^2}\cos\rho\cos\varphi$$

Where ϕ is the phase of the laser

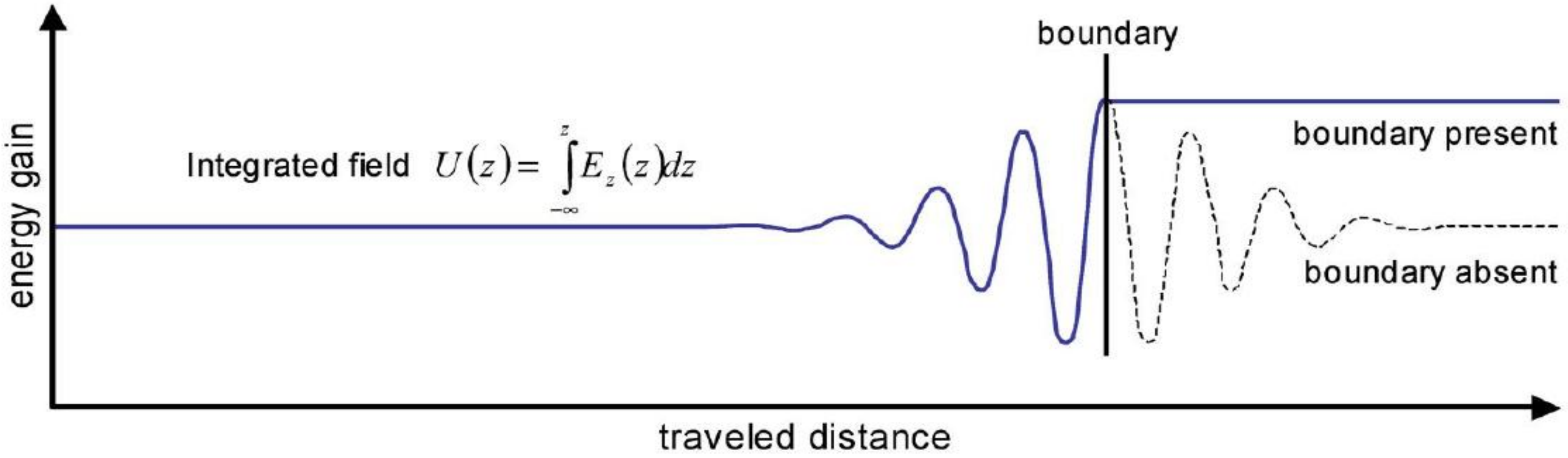

T. Plettner et al., PRL 95, 134801 (2005); PRSTAB 8, 121301 (2005)

Semi-vacuum

TABLE I. Laser and electron beam parameters of the LEAP experiment.

Laser beam parameters	
Wavelength λ	800 nm
Waist FWHM spot size	110 μm
FWHM pulse duration	2–4 psec
Crossing angle α	3–20 mrad
Laser pulse energy	$\frac{1}{2}$ mJ/pulse
Laser repetition rate	1 kHz
Electron beam parameters	
Beam energy	30 MeV
Macro pulse repetition rate	10 Hz (typical)
Micro pulse repetition rate	11.7 MHz
FWHM spot size at the focus	50 μm
FWHM pulse duration	1–2 psec
Initial energy spread	25–30 keV
Charge/bunch at the experiment	~10 pC

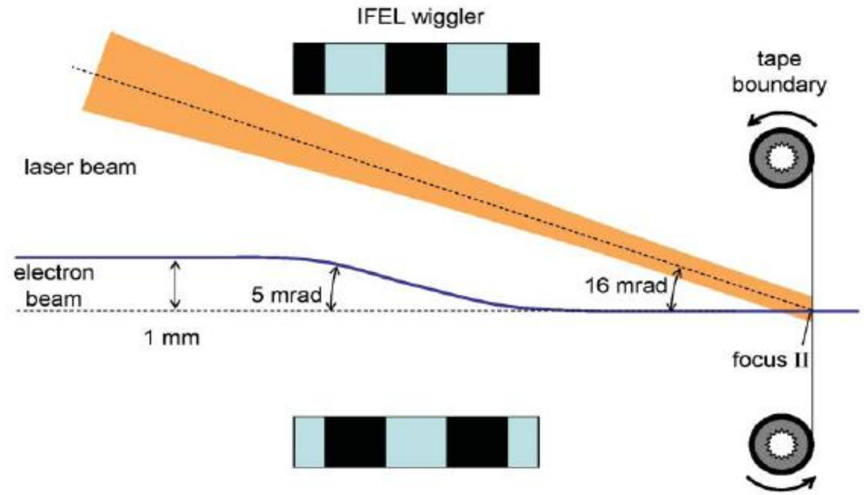

(b)

- •No phase control, expect to see increased energy spread
- • use FEL radiation for timing signal

a) simulated energy profiles

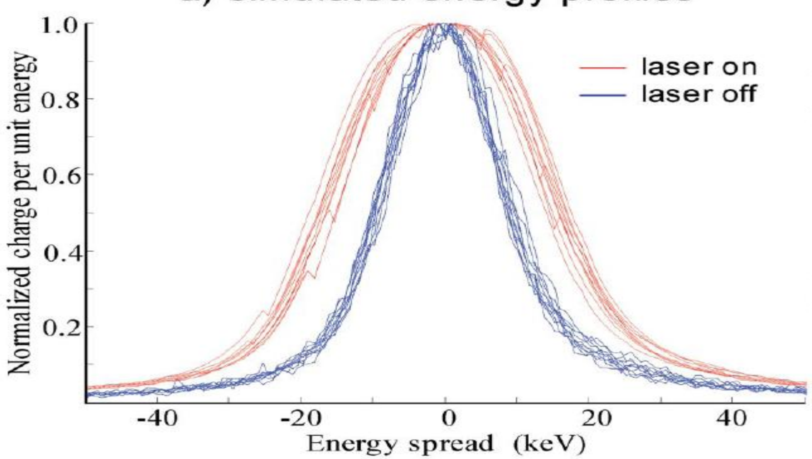

b) simulated laser time scan

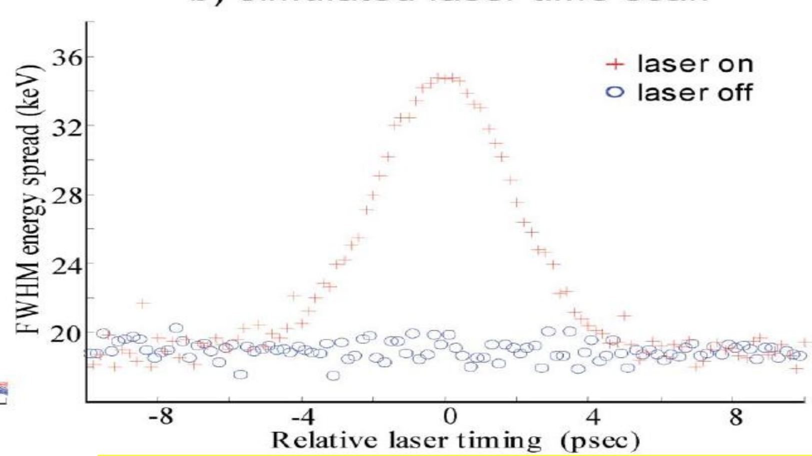

T.

T Plettner et al., PRL 95, 134801 (2005); PRSTAB 8, 121301 (2005)

Semi-vacuum

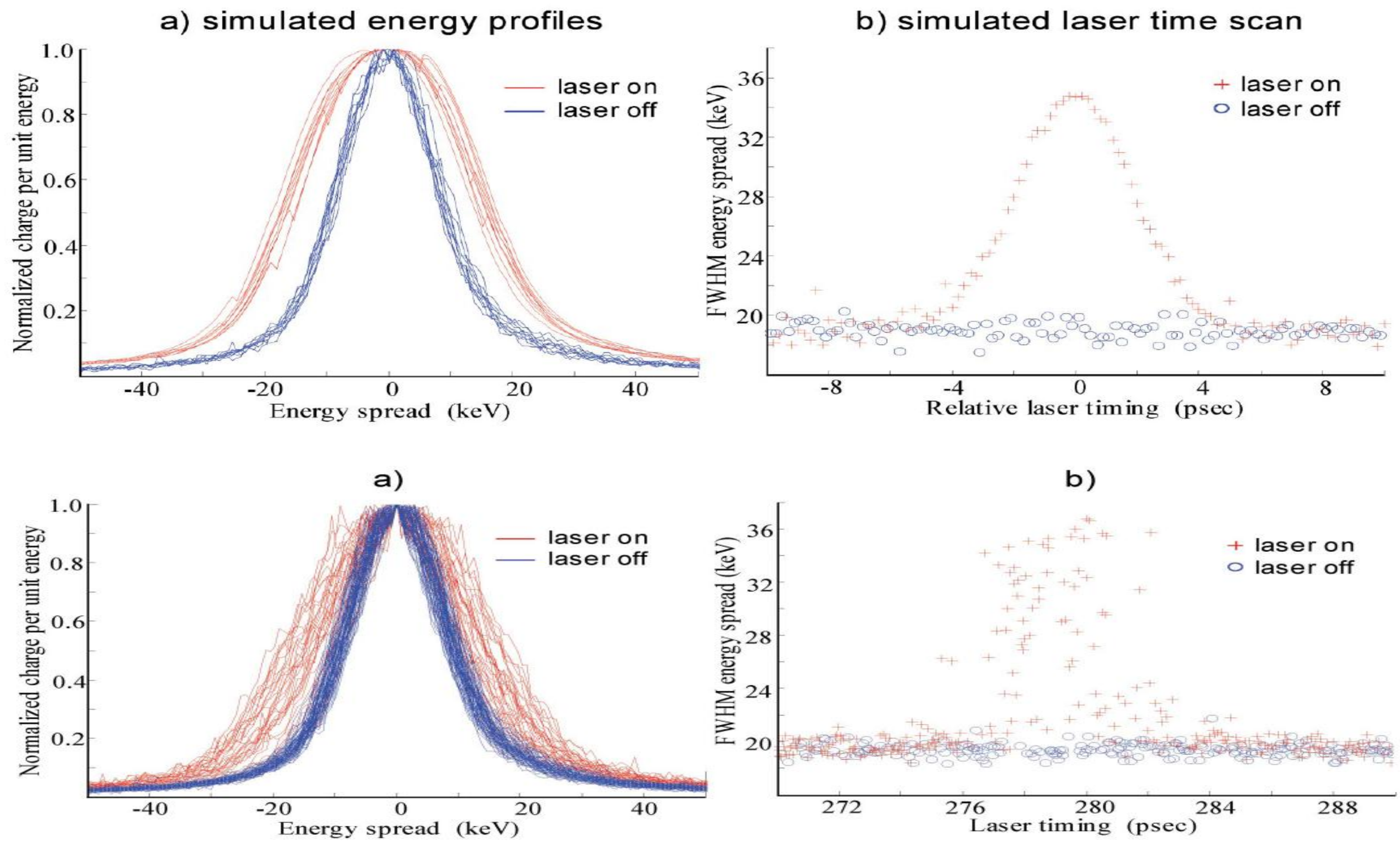

FIG. 8. (Color) (a) Experimentally observed laser-driven energy modulation near the condition of optimum temporal overlap. (b) Laser time scan showing the FWHM energy spread of the electron beam.

T. Plettner et al., PRL 95, 134801 (2005); PRSTAB 8, 121301 (2005)

Plasma wake parameters

plasma oscillations

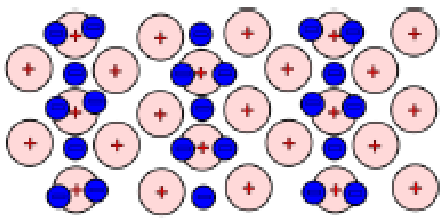

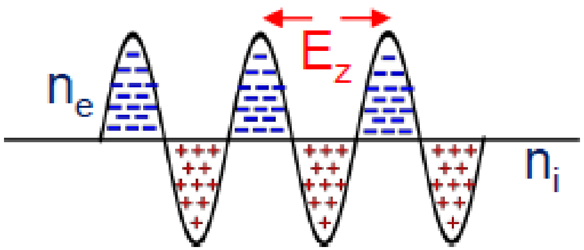

• If you create a charge displacement, it will propagate with a frequency $\omega_p = (4\pi n_0 e^2 / m_e)^{1/2}$ $\lambda_p = 2\pi / \omega_p$

$$\boxed{\lambda_p(\mu\text{m}) \simeq 3.3 \times 10^{10} / \sqrt{n_0(\text{cm}^{-3})}}$$

• axial fields can reach $E_0 = c m_e \omega_p / e$

$$\boxed{E_0(\text{V/m}) \simeq 96\sqrt{n_0(\text{cm}^{-3})}}$$

cold nonrelativistic wave breaking field linear regime (a0<1)

• in nonlinear regime fields can reach

$$\boxed{E_{\text{WB}} = \sqrt{2}(\gamma_p - 1)^{1/2} E_0}$$

nonlinear regime (a0>1)

where $\gamma_p = (1 - v_p^2 / c^2)^{-1/2}$

and v_p is the phase velocity of the plasma wave, which is ~ equal to the group velocity of the laser pulse

$$\beta_p \approx \beta_g / (1 + |\zeta| \lambda_p^{-1} d\lambda_p / dz)$$

$$\gamma_p \approx (1 - v_g^2 / c^2)^{-1/2} = \omega\ / \omega_p$$

$$@ n_0 = 10^{18}\,\text{cm}^{-3}: \quad \text{E}_0 = 96\,\text{GV/m}, \ \lambda_p = 33\,\text{um}$$

Plasma parameters

- Plasma refractive index $$\eta = \sqrt{1 - \frac{\omega_p^2}{\omega^2}}$$

$\omega_p > \omega \longrightarrow \eta$ Plasma refractive index becomes imaginary
$\rightarrow$ Plasma becomes not transparent
$\rightarrow$ Light will reflected by the plasma (like a mirror)

- Critical density $$n_c[cm^{-3}] = \frac{m_e \omega^2}{4\pi\, e^2} \approx \frac{1.1\times 10^{21}}{\lambda[\mu m]^2}$$

$\lambda = 0.8\ \mu m \qquad n_c = 1.7\cdot 10^{21}\ cm^{-3}$ $\rightarrow$ ~ 35 bar Helium gas

$\omega_p > \omega,\ n_p > n_c$ Overdense plasma

$\omega_p < \omega,\ n_p < n_c$ Underdense plasma
$\rightarrow$ Regime for laser electron acceleration

Plasma Wake

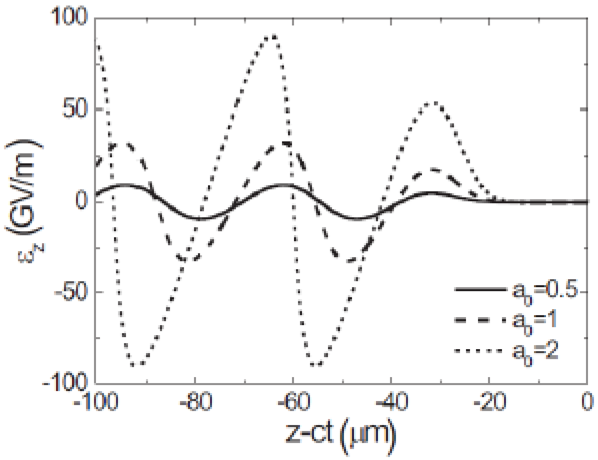

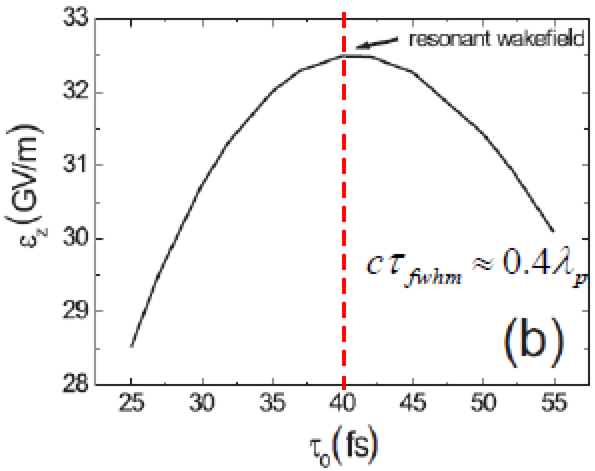

- The amplitude of wakefield increases with increasing the laser intensity
- Linear regime: the wakefield has a sinusoidal shape
- Non-linear regime: the wakefield becomes steeper
- Plasma wavelength increases with increasing the laser intensity
- The resonance occurs when the driver laser length is ~ 0.4 λ_p

Arie Irman LA3NET 2012

Wake-field 'snapshots'

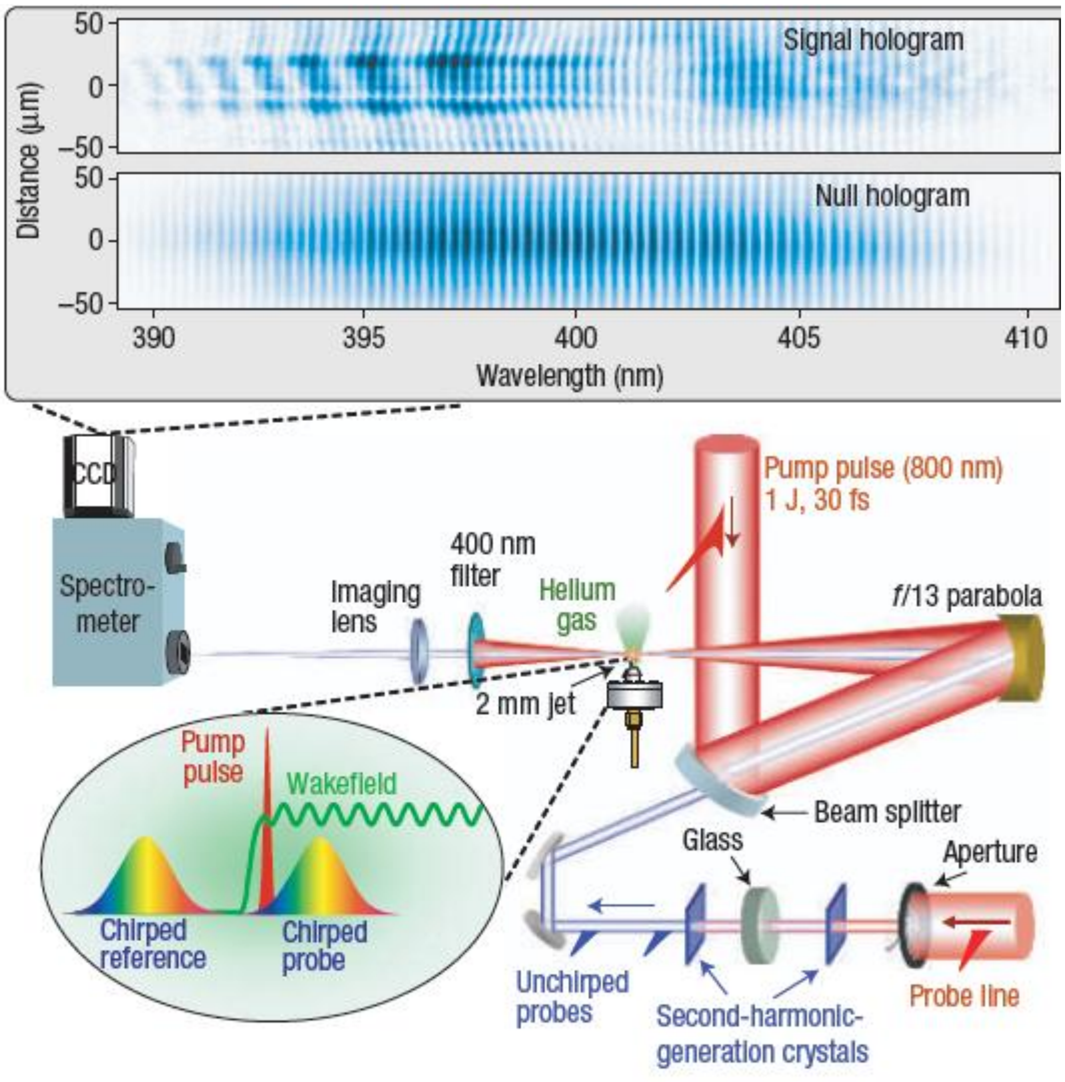

Matlis et al, Nature Phys 2, 749 (2002)

‘Snapshot’ in Nonlinear regime

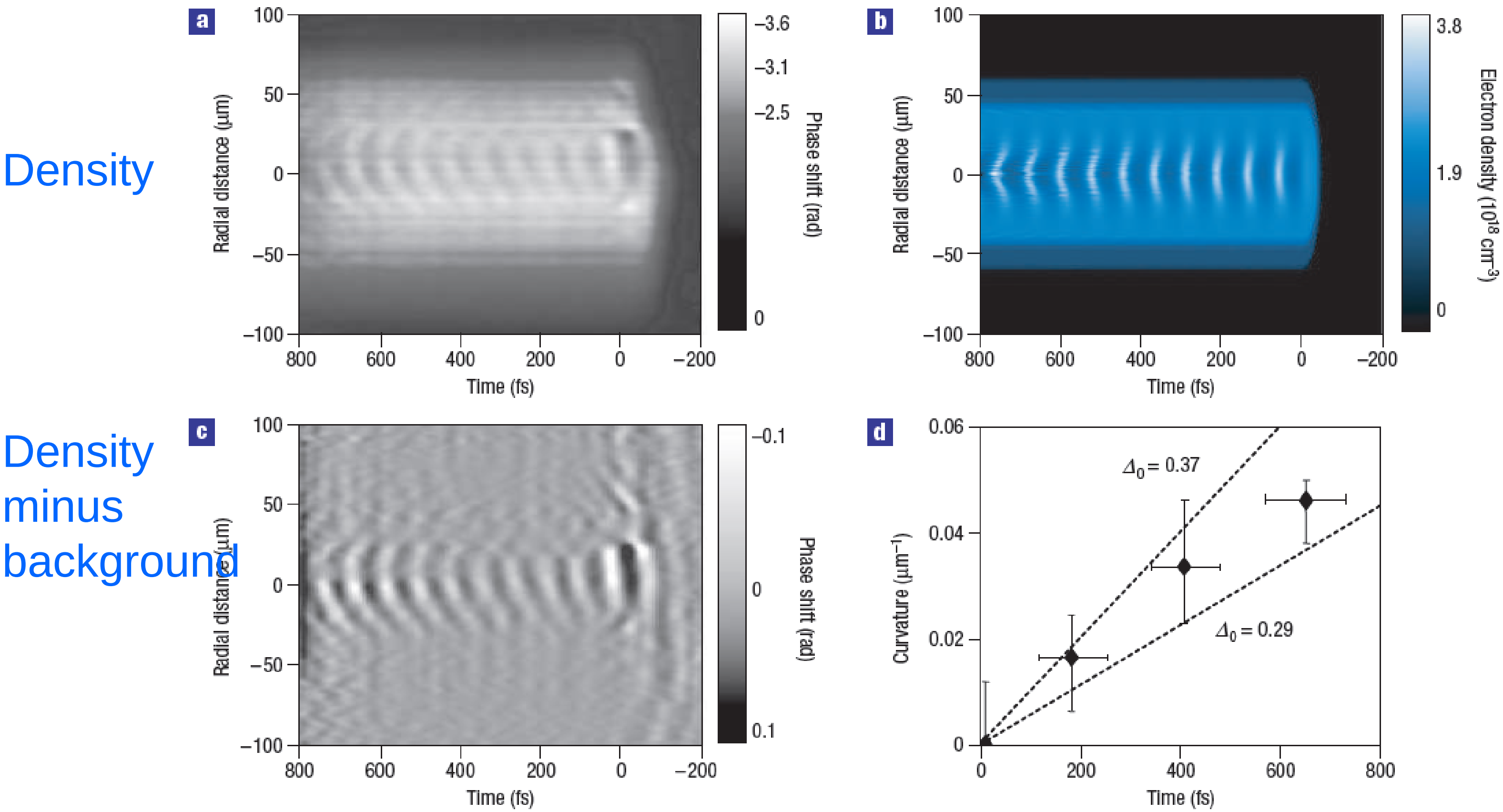

Figure 3 Strongly driven wake with curved wavefronts. a, Probe phase profile $\Delta\phi_{pr}(r,\zeta)$ for an ~30 TW pump, $\bar{n}_e^{max} = 2.2 \times 10^{18}$ cm^{-3} in the He^{2+} region. **b**, Simulated density profile $n_e(r,\zeta)$ near the jet centre. **c**, Same data as in **a**, with the background $\bar{n}_e$ subtracted to highlight the wake. **d**, Evolution of the reciprocal radius of wavefront curvature behind the pump (data points), compared with calculated evolution (dashed lines) for indicated wake potential amplitudes. Each data point (except at $\zeta = 0$) averages over three adjacent periods. The horizontal error bars extend over the three periods averaged, and the vertical error bars extend over the range of fitted curvature values averaged.

As electron oscilation on the axis becomes relativistic, the plasma wave phase velocity there decreases, causing the plasma wavefront to curve

Matlis et al, Nature Phys 2, 749 (2002)

'Snapshot' in linear regime

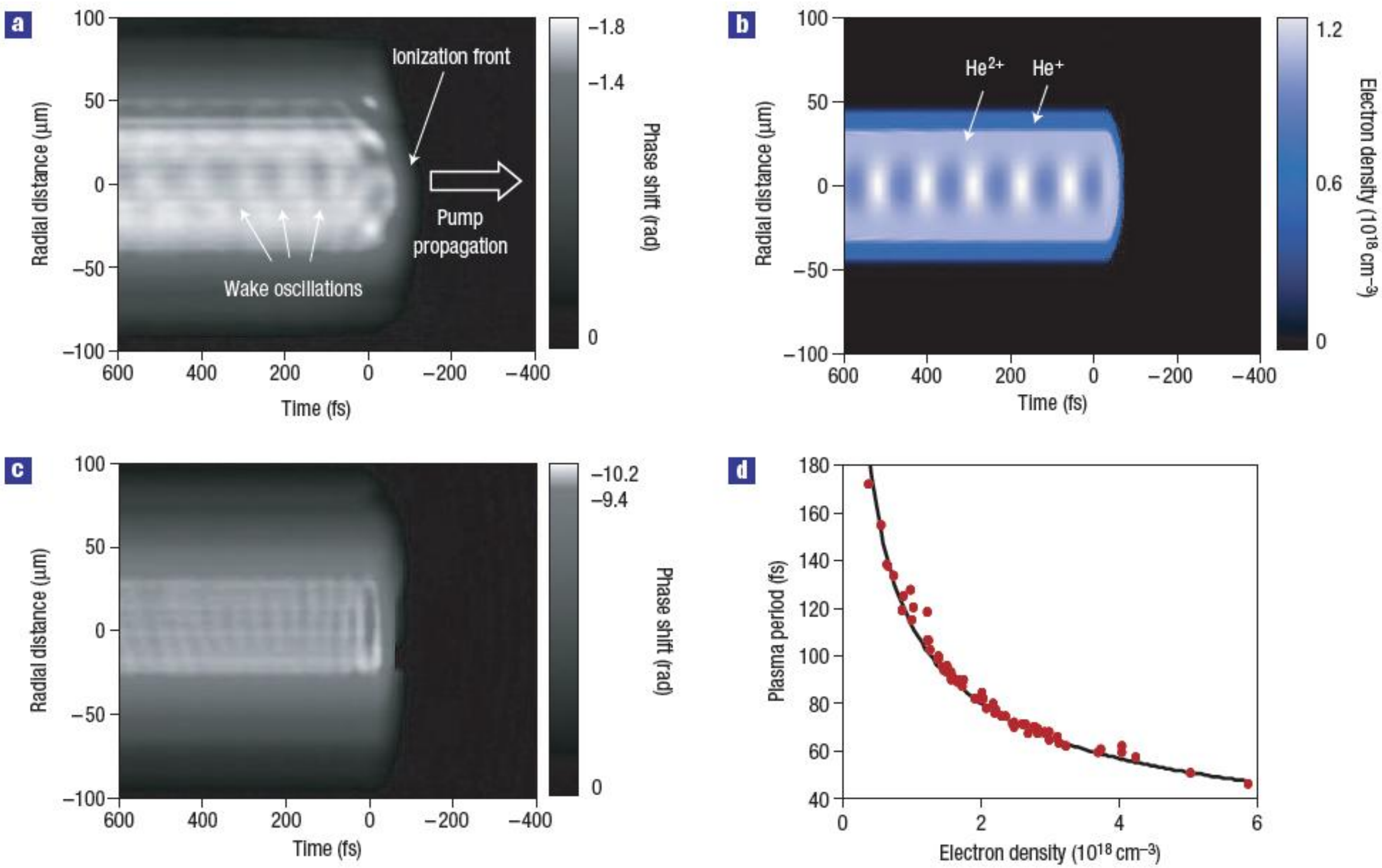

Figure 2 Small-amplitude wakes with flat wavefronts. a, Probe phase-shift profile $\Delta\phi_{pr}(r,\zeta)$ produced by an ~10 TW, 30 fs pump centred at zero on the horizontal scale, electron density $\bar{n}_e^{max} = 0.95 \times 10^{18}$ cm^{-3} in the He^{2+} region. **b**, Simulated wake density profile $n_e(r,\zeta)$ near the jet centre produced by an 11 TW linearly polarized pump. **c**, Same as in **a**, but $\bar{n}_e^{max} = 5.9 \times 10^{18}$ cm^{-3}. **d**, Wake period versus $\bar{n}_e^{max}$, compared with theoretical curve.

Matlis et al, Nature Phys 2, 749 (2002)

How to get the electrons in

- bunch must be short relative to λ_p; λ_p~30-100 um
- Need to place at the right position and velocity for optimal gain over maximal dephasing length

Electron Injection

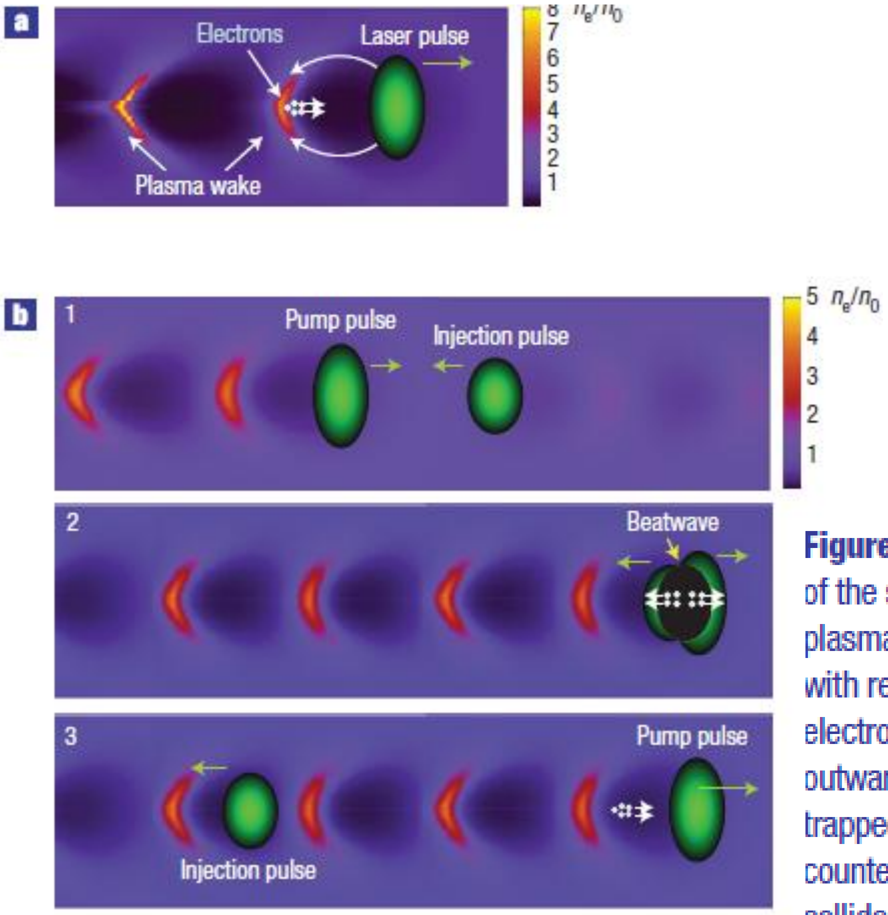

Figure 1 Injection schemes in laser–plasma accelerators. **a**, A schematic diagram of the self-injection mechanism in the bubble regime. The figure represents a plot of plasma electron density behind the laser pulse. The plasma wake is highly nonlinear with regions where electrons have been evacuated (black) and regions where electrons accumulate (yellow). The arrows show how electrons are deflected outward and then accumulate at the back of the wakefield, where some of them are trapped and accelerated. **b**, Schematic diagrams of the injection mechanism in the counterpropagating colliding pulse scheme. (1) The two laser pulses have not collided yet; the pump pulse drives a strong plasma wake, although less nonlinear than in the bubble regime case. (2) The pulses collide and their interference sets up a beatwave that preaccelerates electrons. (3) Some of the preaccelerated electrons are trapped and further accelerated in the wake.

V. Malka, Nature Phys 4, 447 (2008)

Electron injection, blowout/bubble regime

PIC calculation

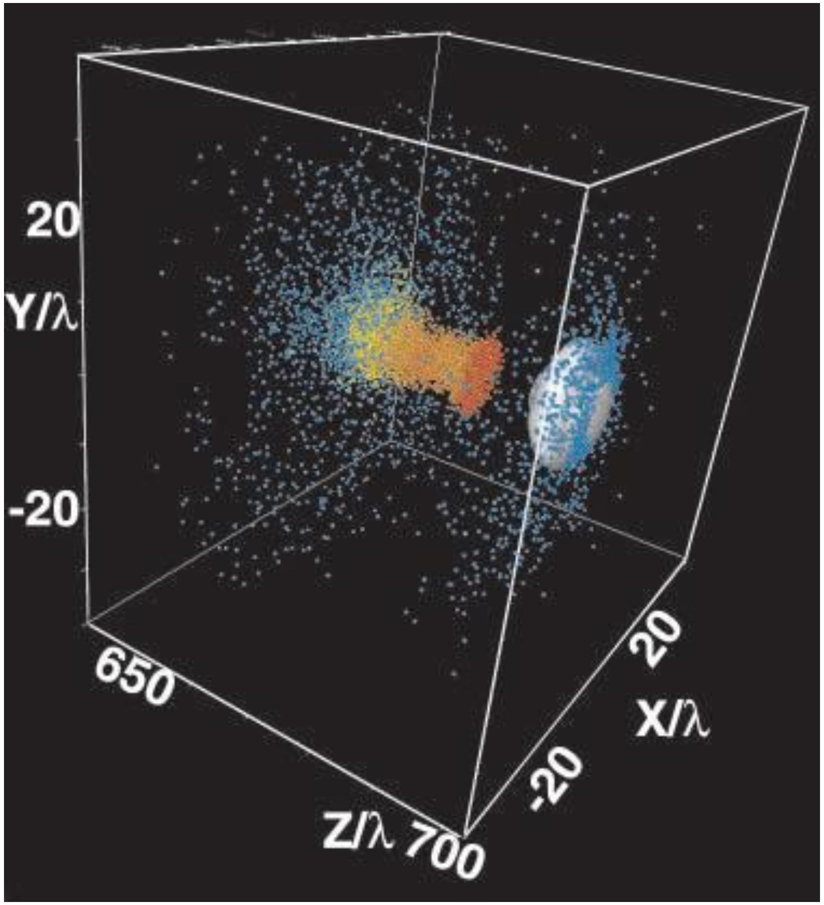

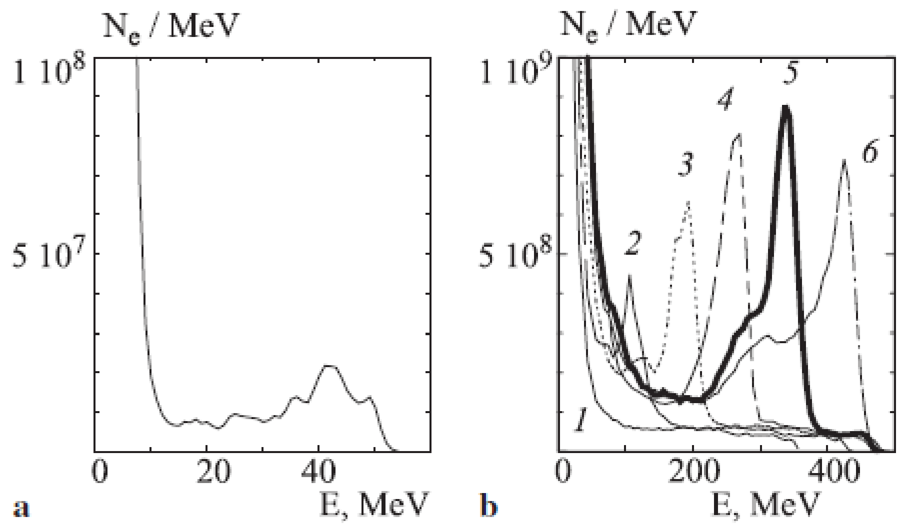

FIGURE 2 Spectra of accelerated electrons: **a** final spectrum of the case of Fig. 1; **b** the case of the 33-fs, 12-J laser pulse, time evolution of the energy spectrum: (1) $ct/\lambda = 350$, (2) $ct/\lambda = 450$, (3) $ct/\lambda = 550$, (4) $ct/\lambda = 650$, (5) $ct/\lambda = 750$ corresponding to Figs. 3, 4, and 5, (6) $ct/\lambda = 850$

Pukhov & Meyer-ter-Vehn, Appl. Phys. B 74, 355–361 (2002)

FIGURE 3 The case of a 12-J, 33-fs laser pulse after propagating $z/\lambda = 690$ in 10^{19} cm^{-3} plasma. 3D perspective view of hot electron distribution. Each 100th electron above 10 MeV is shown as a *dot* colored according to its energy. The *white disc* shows the laser-intensity surface at $I = 10^{19}$ W/cm^2

Electron injection, colliding pulse

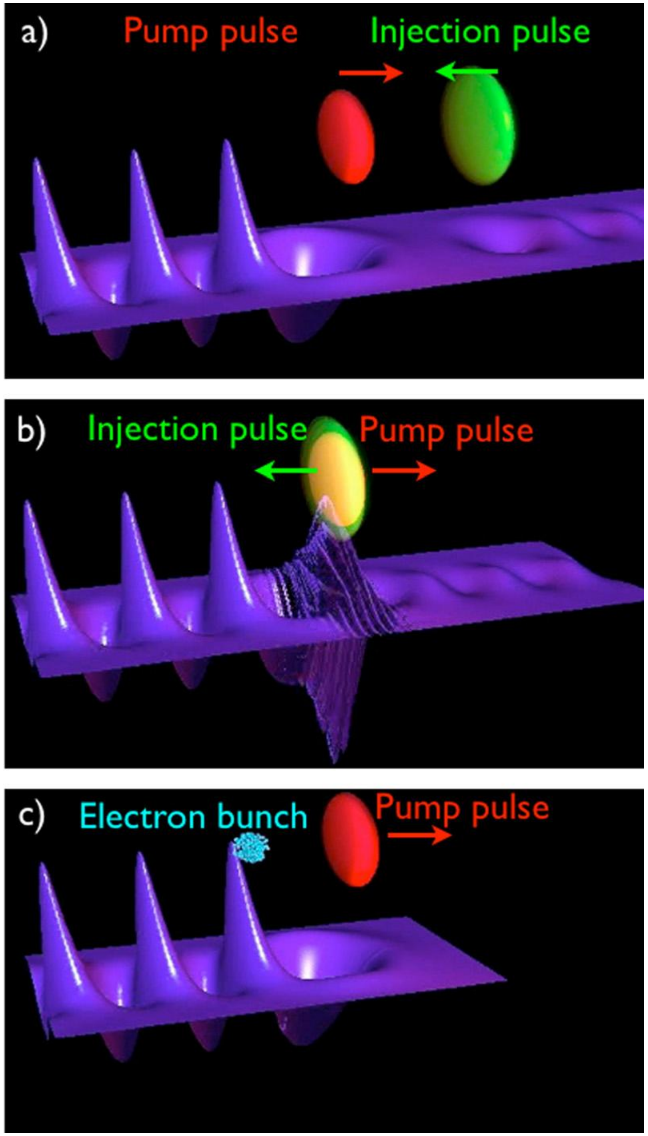

FIG. 6. Scheme of principle of the injection with colliding laser pulses:
(a) the two laser pulses propagate in opposite direction,
(b) during the collision, some electrons get enough longitudinal momentum to be trapped by the relativistic plasma wave driven by the pump beam,
(c) trapped electrons are then accelerated in the wake of the pump laser pulse.

V Malka, Phys. Plasmas 19, 055501 (2012)

Beam loading terminates trapping

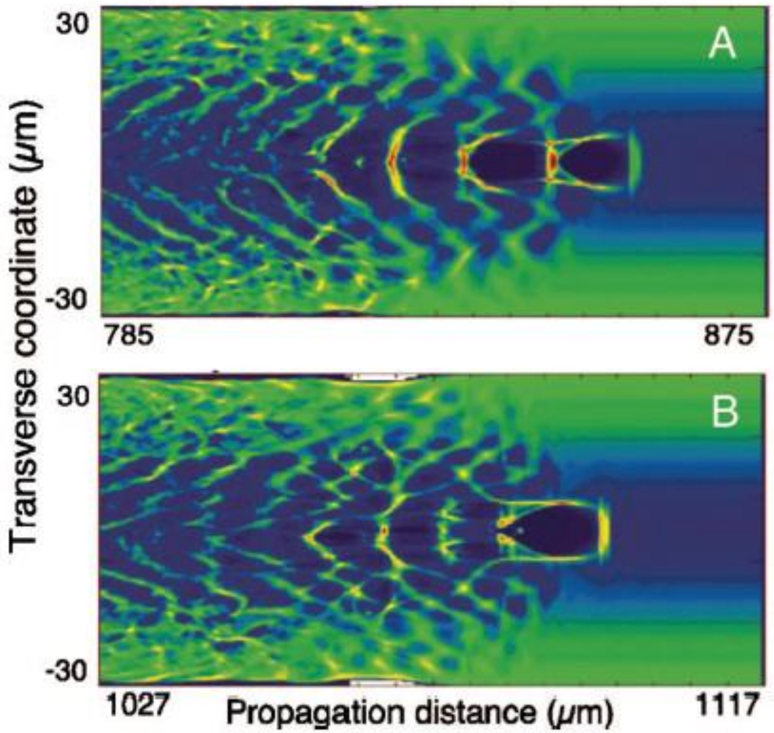

FIG. 42. (Color) PIC simulation of electron density after laser propagation of (a) 875 μm and (b) 1117 μm. (a) The density perturbation just prior to self-trapping in the first bucket behind the laser. (b) A trapped electron bunch is damping the wake and suppressing further trapping, isolating the initial bunch in phase space. From Geddes *et al.*, 2005b.

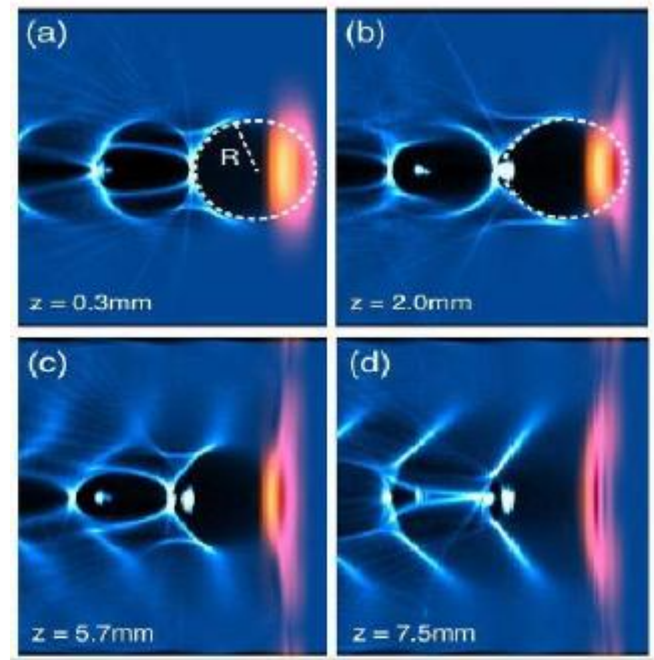

Lu, W., *et al*, PRSTAB 10,061301(2007)

E. Esarey et al, RevModPhys 81, 1229 (2009)

LLNL Staged Accleration to 0.5 GeV

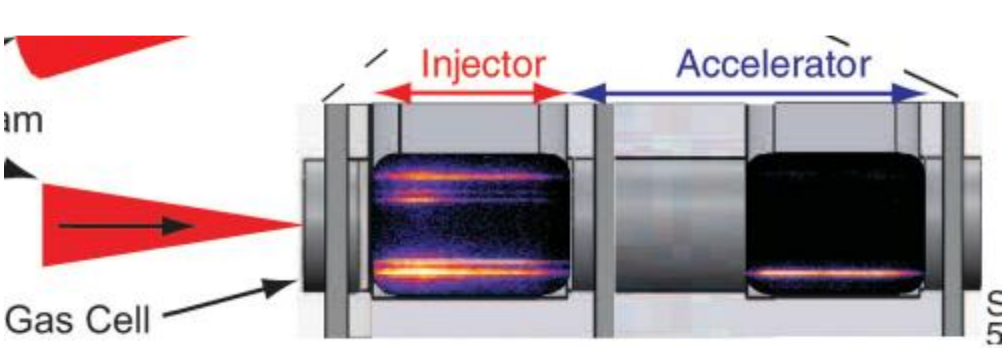

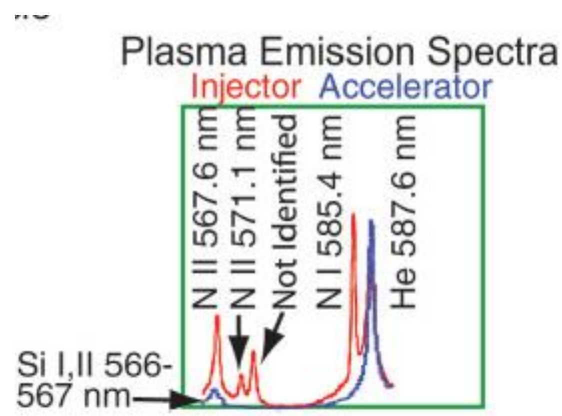

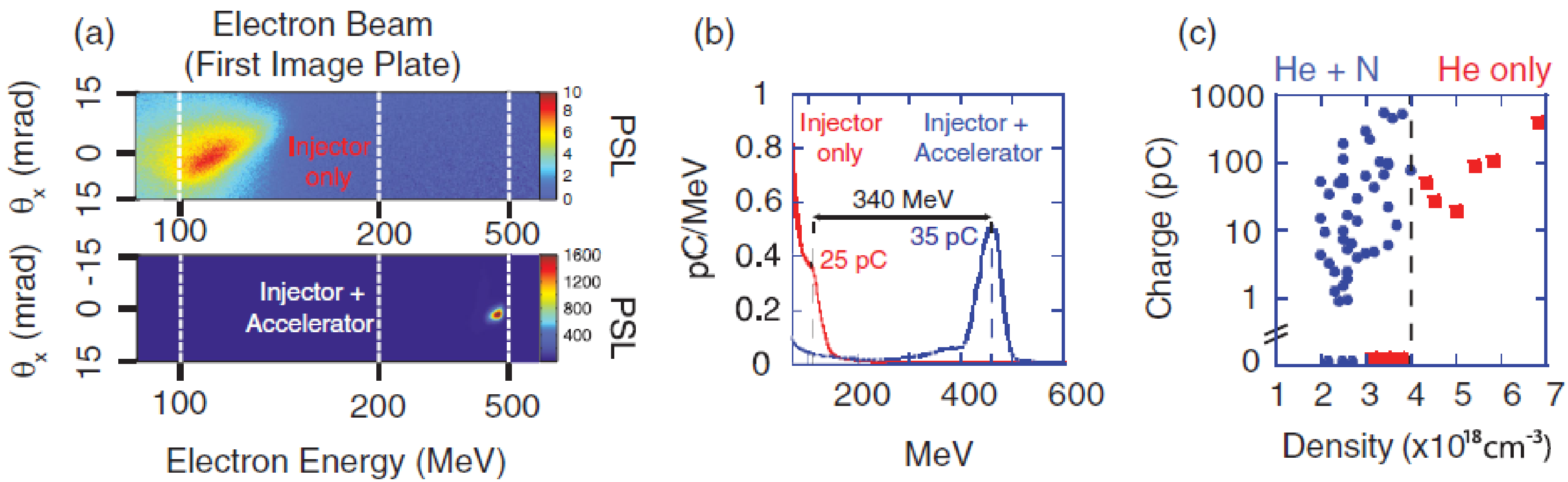

- Stage 1 cell ‘seeded’ with N2
- no self-trapping in He stage 2 at given density

Pollock et al., Phys. Rev. Lett. 107, 045001 (2011).

Staged Accleration to 0.5 GeV

35 pC, <5% energy spread

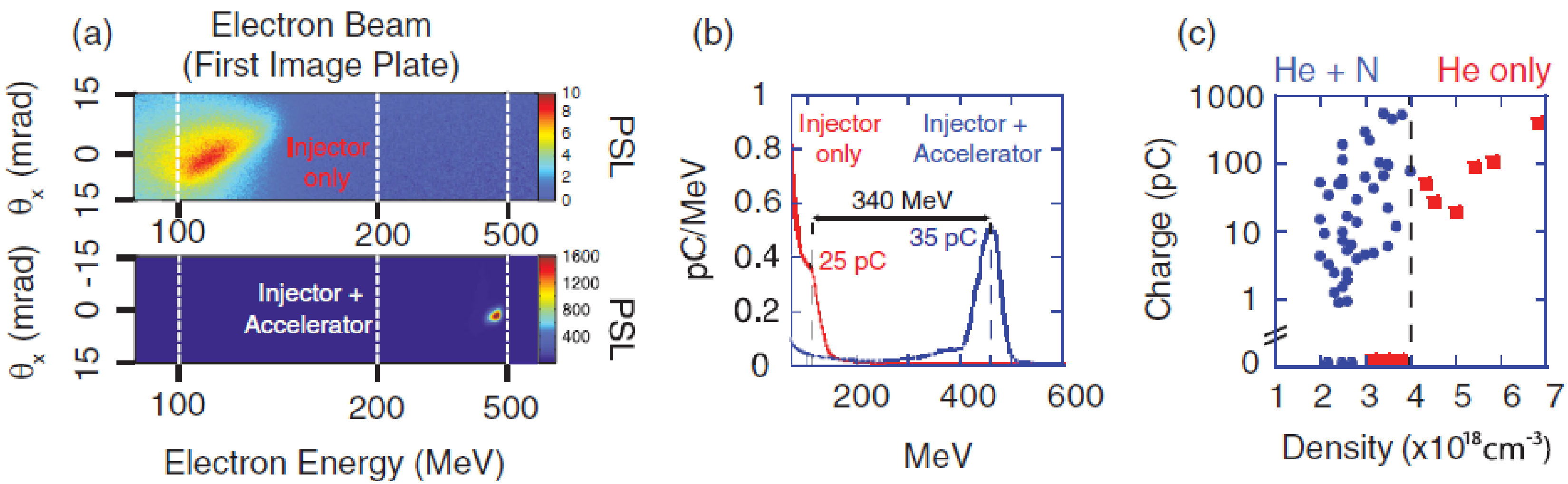

FIG. 2 (color). (a) Magnetically dispersed electron beam images from a 4 mm injector-only gas cell (top) and the 8 mm two-stage cell (bottom). (b) Electron spectra above 70 MeV for the 8 mm two-stage injector-accelerator cell (blue curve) filled to an electron density of 3×10^{18} cm^{-3} in each stage for a coupled laser power of 40 TW and the 4 mm injector-only cell (red curve) filled to an electron density of 3.4×10^{18} cm^{-3} for a coupled laser power of 50 TW. The injector gas fill in each case is 99.5% He and 0.5% N_2, and the total charge is indicated for each spectrum. (c) The total observed charge above 70 MeV for injector gas fills of pure He (red squares) and 99.5% He with 0.5% N_2 (blue circles) for coupled laser powers between 30 and 60 TW.

Pollock et al., Phys. Rev. Lett. 107, 045001 (2011).

LBNL capillary discharge & density tailoring

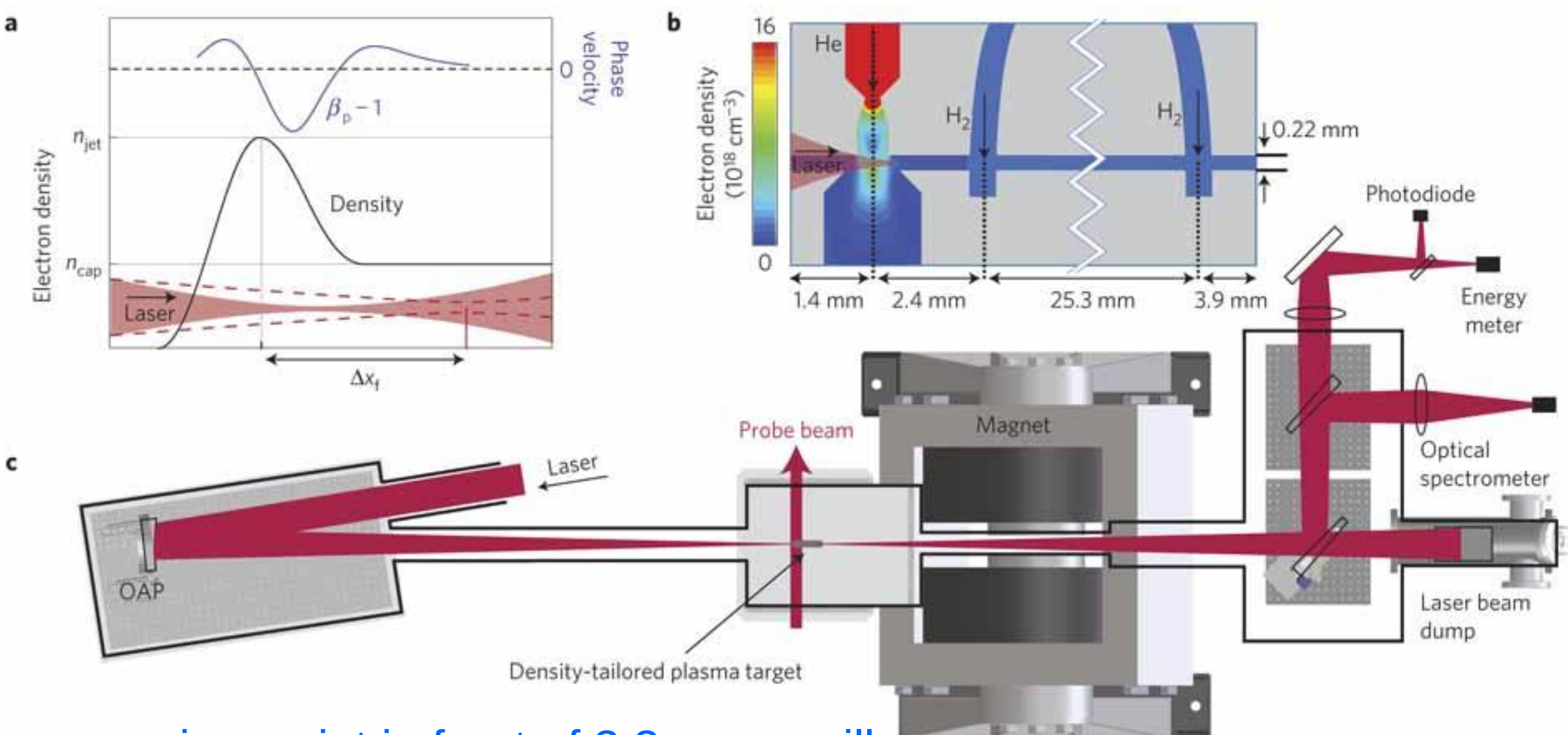

- supersonic gas jet in front of 3.3 mm capillary discharge
- tailor density so that injection terminates
    - sub-mm plasma in jet
    - self focusing -> v_{ph} slowing to facilitate injection, then shut off self-focusing
- 30% pump depletion, plenty left for wake generation in capillary discharge waveguide
- 'tune' with focal position Δx_f

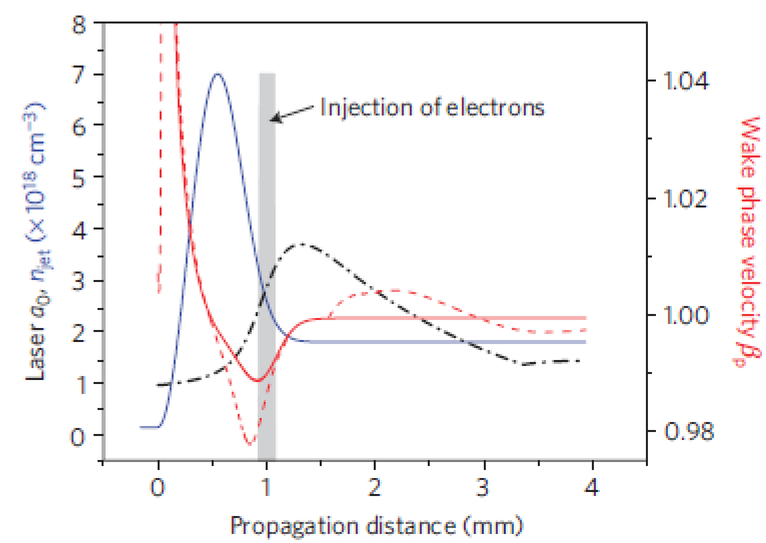

Gonsalves et al Nature Phys 7, 862 (2011)

LBNL capillary discharge & density tailoring

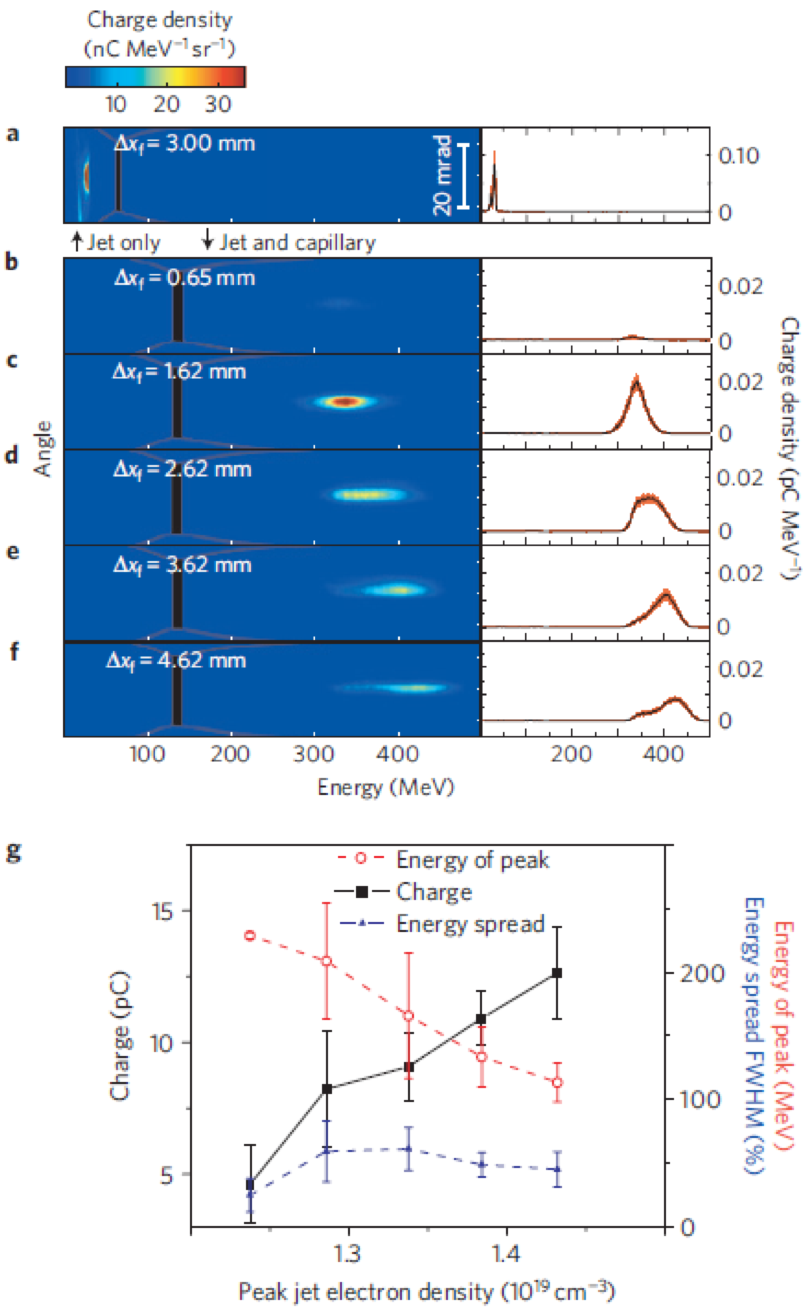

Figure 2 | Electron-beam data from both the gas jet and the density-tailored plasma target, demonstrating the post-injection acceleration in the capillary structure and the control over electron-beam properties afforded by the density-tailored approach. a–f, Averaged magnetic spectrometer images from 20 consecutive shots. The black shaded areas in each image represent the regions not covered by the spectrometer cameras. Lineouts of the mean (black curve) and the standard deviation (red area) are on the right of each image. The LPA in **a** consisted only of a helium gas jet with peak electron density $n_{jet} \approx 7 \times 10^{18}$ cm^{-3} and length (FWHM) 0.75 mm. For **b–f** a helium gas jet with $n_{jet} \approx 7 \times 10^{18}$ cm^{-3} and length (FWHM) 0.55 mm was coupled to a capillary with density $n_{cap} \approx 1.8 \times 10^{18}$ cm^{-3} for various focal locations Δx_f. **g**, The charge (squares), energy (circles) and energy spread (triangles) as a function of peak jet density for $\Delta x_f = 0.62$ mm at capillary density $n_{cap} \approx 1.2 \times 10^{18}$ cm^{-3}. The error bars correspond to the standard deviation of the data.

Gonsalves et al Nature Phys 7, 862 (2011)

Living with the energy spread: FEL with TGU

(Free Electron Laser with Transverse Gradient Undulator)

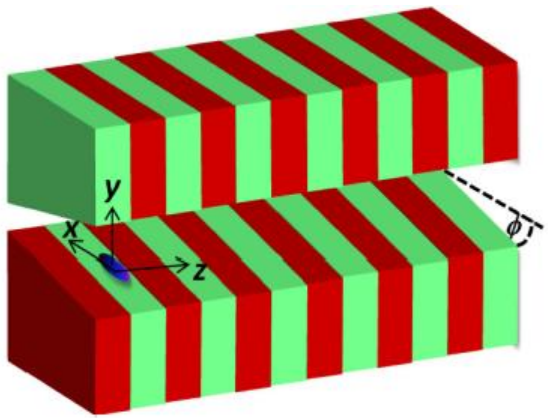

FIG. 1 (color online). Transverse gradient undulator by canting the magnetic poles. Each pole is canted by an angle ϕ with respect to the xz plane. The higher energy electrons are dispersed to the higher field region (positive x) to match the FEL resonant condition.

- Progress towards LPA beams of 1 GeV, 10 kA, 0.1 um emittance
- energy spread an issue for FELs
- transversely disperse e bunch and compensate with a canted-pole wiggler
- at early stage of numerical feasibility studies

$$\lambda_r = \frac{\lambda_u}{2\gamma_0^2}\left(1 + \frac{K_0^2}{2}\right).$$

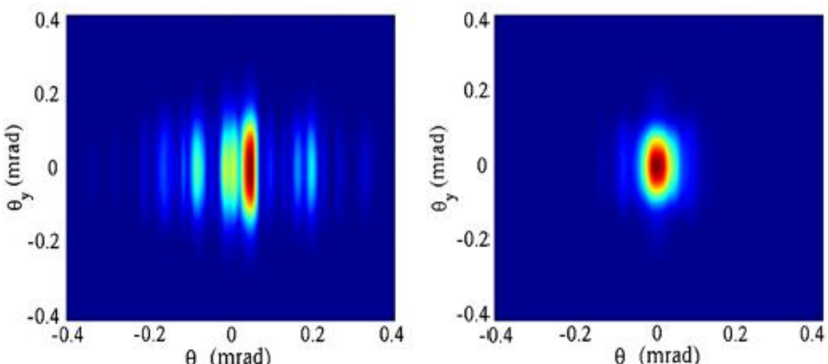

(a)SASE. (b)Seeded.

FIG. 5 (color online). Trasverse mode pattern for a SASE and a seeded FEL at 31 nm based on the THUNDER TGU.

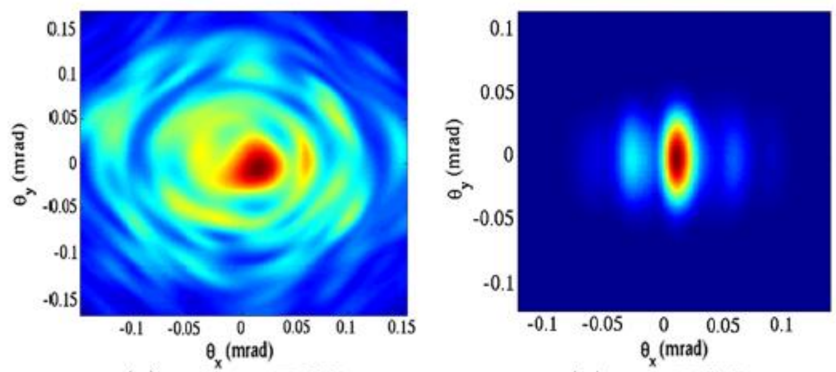

(a)without TGU. (b)with TGU.

FIG. 8 (color online). Trasverse mode pattern for a SASE FEL at 3.9 nm.

Huang et al PRL 109, 204801 (2012)

Issues for the future

- Repetition rate

- Stability in plasma and laser propagation

- Computational issues for simulations of extended accelerators
    - need high temporal and spatial resolution for laser, plasma wave, self-injection, and trapping, but long propagation lengths

- Average power: for useful luminosity, need kHz x nC x TeV = MW
    - laser-plasma coupling @ 1% energy spread = 1%
        - what might be some problems re-using the laser pulse?*
    - laser wallplug efficiency = 1% (could improve)
    - 10 GW !
    - laser-seeded e-bunch-driven plasma ERL? (back to big structures)*

- Propagation effects, laser coupling effects etc over "long" distances

* jump-offs for discussion

V Malka, Phys. Plasmas 19, 055501 (2012)
E Esarey et al, RevModPhys 81, 1229 (2009)